On the possibility and necessity of space-time unified descriptions for electromagnetic Form Factors

R. Baldini Ferroli

Centro Studi e Ricerche e Museo Storico della Fisica "Enrico Fermi", Roma
and INFN Laboratori Nazionali di Frascati, Frascati, Italy

S. Pacetti

Dipartimento di Fisica, Università di Perugia, and INFN, Sezione di Perugia, Italy

Electromagnetic form factor represent the only experimental probe for non-perturbative quantum chromodynamics. They allow to access information on the parton structure of hadrons in terms of energy-dependent couplings to photons. New sets of data, mainly in time-like region, coming from flavor-factories, make possible more accurate analyses which require a deeper understanding of hadron structure and more sophisticated fitting techniques.

Keywords: .

1. Introduction

Electromagnetic form factors (FFs) describe modifications of pointlike photon-hadron vertices due to the structure of hadrons. The photon, interacting with single elementary charges, the quarks, represents a powerful probe for the internal structure of composite particles. Furthermore, being the electromagnetic leptonic interaction exactly calculable in QED, the dynamical content of each vertex can be easily extract from data.

1.1. *Nucleon Form Factors*

The elastic scattering of an electron by a nucleon $e^-N \to e^-N$ is represented, in Born approximation, by the diagram of fig. 1, in the vertical direction. In this kinematic region the four-momentum of the virtual photon is space-like and hence its squared value is negative: $q^2 = -2\omega_1\omega_2(1-\cos\theta_e) \leq 0$, being $\omega_{1(2)}$ the energy of the incoming (outgoing) electron and θ_e the scattering angle.

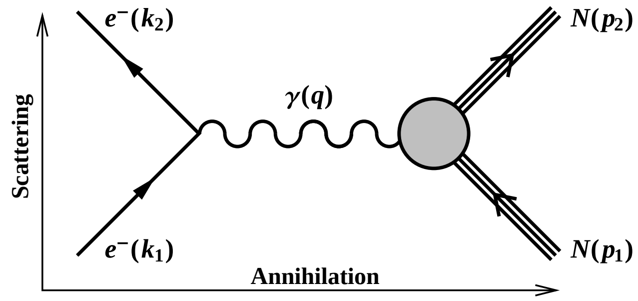

Fig. 1. One-photon exchange Feynman diagram for scattering $e^-N \to e^-N$ and annihilation $e^+e^- \to N\overline{N}$.

The same diagram of fig. 1, but in the horizontal direction, represents the annihilation $e^+e^- \to N\overline{N}$ or $N\overline{N} \to e^+e^-$. For these processes the four-momentum q is time-like, in fact: $q^2 = (2\omega)^2 \geq 0$, where $\omega \equiv \omega_1 = \omega_2$ is the common value of the lepton

energy in the e^+e^- center of mass frame (CM).
The Feynman amplitude for the elastic scattering is

$$\mathcal{M} = \frac{1}{q^2}[e\,\overline{u}(k_2)\gamma^\mu u(k_1)][e\,\overline{U}(p_2)\Gamma_\mu(p_1, p_2)U(p_1)]\,, \tag{1}$$

where the four-momenta follow the labelling of fig. 1, u and U are the electron and nucleon spinors, and Γ^μ is a non-constant matrix which describes the nucleon vertex. Using gauge and Lorentz invariance the most general form of such a matrix is[1]

$$\Gamma^\mu = \gamma^\mu F_1(q^2) + \frac{i\sigma^{\mu\nu}q_\nu}{2M}F_2(q^2)\,, \tag{2}$$

where M is the nucleon mass. Γ^μ depends on two Lorentz scalar functions of q^2, $F_1(q^2)$ and $F_2(q^2)$ called Dirac and Pauli FFs, they describe the non-helicity-flip and the helicity-flip part of the hadronic current respectively. Normalizations at $q^2 = 0$ follow from total charge and magnetic moment conservation and are

$$F_1(0) = Q_N\,, \qquad F_2(0) = \kappa_N\,, \tag{3}$$

where Q_N is the electric charge (in units of e) and κ_N the anomalous magnetic moment (in units of the Bohr magneton μ_B) of the nucleon N.
Other pairs of FFs can be defined as combinations of F_1 and F_2, of particular interest are the so-called Sachs FFs G_E and G_M[2] that can be obtained from the hadronic current written in a special frame, i.e. the Breit frame. Indeed in such a frame the transferred four-momentum q is purely space-like: $q = (0, \vec{q})$ and the nucleon momentum, during the scattering, passes from $-\vec{q}/2$ to $+\vec{q}/2$. Under these conditions the hadronic current gets the standard form of an electromagnetic four-current, i.e. the time and the space-component are Fourier transformations of a charge density and a current density respectively, i.e.:

$$\begin{cases} \rho_q = J^0 = e\left[F_1 + \dfrac{q^2}{4M^2}F_2\right] \\[2ex] \vec{J}_q = e\,\overline{U}(p_2)\vec{\gamma}U(p_1)\,[F_1 + F_2]\,. \end{cases} \tag{4}$$

As a consequence, Sachs electric and magnetic FFs are defined through the combinations

$$\begin{cases} G_E = F_1 + \dfrac{q^2}{4M^2}F_2 \\[2ex] G_M = F_1 + F_2\,. \end{cases} \tag{5}$$

At the time-like production threshold $q^2 = 4M^2$, assuming only S-wave contribution, that is, a non singular behavior for F_1 and F_2, the Sachs FFs are equal each other, i.e.:

$$G_E(4M^2) = G_M(4M^2)\,. \tag{6}$$

The normalization of the Sachs FFs at $q^2 = 0$ follows from their interpretation in terms of Fourier transformations of charge and magnetic moment distributions and it is

$$G_E(0) = Q_N\,, \qquad G_M(0) = \mu_N\,, \tag{7}$$

where $\mu_N = Q_N + \kappa_N$ is the nucleon magnetic moment in units of the Bohr magneton μ_B.

1.2. *Time-like region, analytic properties and asymptotic behavior*

Analyticity of nucleon FFs as functions of q^2 is guaranteed by the microcausality[3] and the unitarity, implemented through the optical theorem,[4] defines discontinuities in the q^2 complex plane. Nucleon FFs are real in the space-like region, i.e. for $q^2 \le 0$. In the time-like region, for positive q^2, the photon carries enough virtual mass to couple with intermediate, on-shell states.
Therefore, using the optical theorem as schematically represented in fig. 2, the imaginary part of the amplitude which describes the coupling of the photon to the nucleon-antinucleon pair can be decomposed as

$$\mathrm{Im}\left[\langle\overline{N}(p_1)N(p_2)|J|0\rangle\right] \sim \sum_n \langle\overline{N}(p_1)N(p_2)|J^\dagger|n\rangle\langle n|J|0\rangle\,, \tag{8}$$

where n runs over all the hadronic intermediate states allowed by conservation laws. The lightest hadronic state to be considered, and hence the first that opens, is the $\pi^+\pi^-$ channel. It follows that the amplitude as well as the FFs, which characterize the q^2 dependence of the nucleon current, acquire an imaginary part different from zero starting from the so-called theoretical threshold

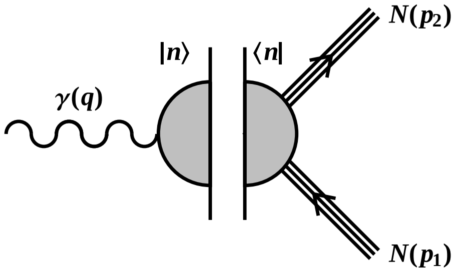

Fig. 2. Spectral decomposition of the time-like nucleon vertex.

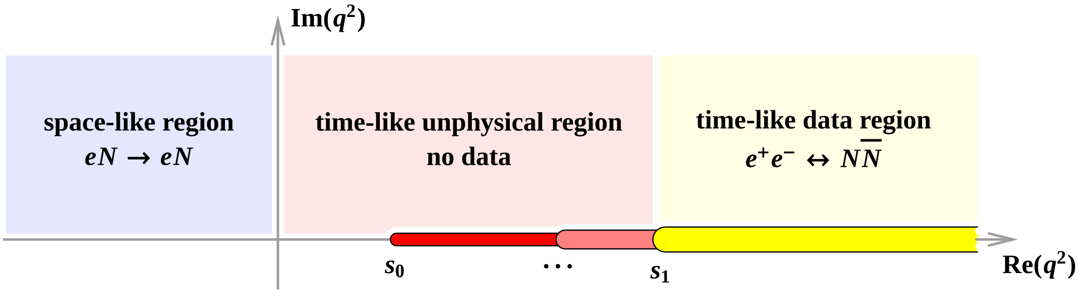

Fig. 3. The q^2 complex plane with the discontinuity on the real axis given by the superposition of all the intermediate-channel cuts.

$s_0 = (2M_\pi)^2$. The FFs are then analytic functions in the whole q^2 complex plane, shown in fig. 3, with a discontinuity cut, over the real axis (time-like region), from s_0 up to infinity.
Such a cut is the superposition of the infinite possible intermediate states that can couple with the virtual photon and produce the final nucleon-antinucleon pair.

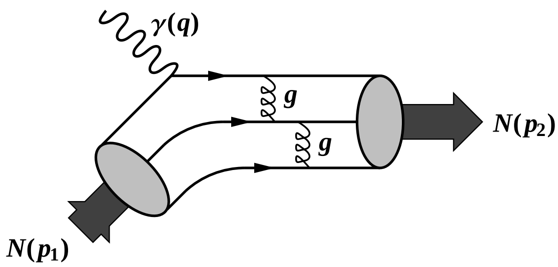

Fig. 4. A photon at large virtuality interacts with the nucleon.

In the framework of perturbative QCD (pQCD), the FF asymptotic behavior in the space-like region, i.e. as $q^2 \to -\infty$, is driven by two principles: the quark counting rule[5] and the hadronic helicity conservation.[6] At asymptotically large values of $-q^2$, the photon has sufficiently large virtuality to see the nucleon made of three collinear quarks, as sketched in fig. 4. To keep the nucleon intact, the momentum transferred by the photon has to be shared among the constituent quarks. The minimal action to be done in order to guarantee the partitioning of q is represented by two gluon exchanges as shown in fig. 4. The corresponding two gluon propagators give the power low $(-q^2)^{-2}$ for the FF. More in detail, for the Dirac and Pauli FFs the asymptotic power laws are

$$\lim_{q^2\to-\infty} F_1(q^2) \sim \left(\frac{1}{-q^2}\right)^2, \qquad \lim_{q^2\to-\infty} F_2(q^2) \sim \left(\frac{1}{-q^2}\right)^3. \tag{9}$$

The Pauli FF $F_2(q^2)$ is connected to the helicity-violating part of the hadronic current and, since the helicity flip involves, at leading order, a further gluon-exchange and hence an additional gluon propagator, the resulting power law is $(-q^2)^{-3}$, as reported in eq. (9). The Sachs FFs, defined in eq. (5), have the same asymptotic power law, i.e.

$$\lim_{q^2\to-\infty} G_{E,M}(q^2) \sim \left(\frac{1}{-q^2}\right)^2. \tag{10}$$

The asymptotic behavior in the time-like region can be inferred from the space-like one invoking the Phragmén-Lindelöf theorem[a].[7] In fact, having that the FFs are regular and bounded in the whole upper half q^2-complex plane ($\mathrm{Im}\, q^2 \geq 0$), the limits along the two lines that define this region, the negative and positive real axes, must be equal, i.e.:

$$\underbrace{\lim_{q^2\to+\infty} G_{E,M}(q^2)}_{\text{time-like}} = \underbrace{\lim_{q^2\to-\infty} G_{E,M}(q^2)}_{\text{space-like}} \sim \left(\frac{1}{|q^2|}\right)^2 . \tag{11}$$

Since in the time-like region FFs are complex, the fact that they vanish as real functions means that the imaginary part vanishes faster than the real one or, in other words, that the phase, as $q^2 \to +\infty$, tends to integer multiples of π radians.

1.3. *Cross sections*

Data on nucleon FFs can be obtained studying angular distributions of differential cross sections for the scattering $e^-N \to e^-N$ and the annihilation $e^+e^- \leftrightarrow N\overline{N}$. In particular, as it is shown in the schematic representation of fig. 3:

- from elastic scattering we gain information on the real values of FFs in the space-like region ($q^2 \leq 0$);
- from annihilation cross sections we extract the moduli of the FFs above the physical threshold $s_1 = (2M)^2$;
- in the remaining energy interval, from $q^2 = 0$ up to $q^2 = s_1$, the so-called "unphysical region", FFs are not experimentally accessible even though, thanks to the analyticity, they are still well defined.

The differential cross section for the elastic scattering $e^-N \to e^-N$ in the laboratory frame, i.e. $p_1 = (M, \vec{0})$, and in Born approximation is

$$\frac{d\sigma}{d\cos\theta_e} = \frac{\pi\alpha^2\omega_2\cos^2\frac{\theta_e}{2}}{2\,\omega_1^3\sin^4\frac{\theta_e}{2}} \left\{ G_E(q^2)^2 - \tau\left[1 + 2(1-\tau)\tan^2\frac{\theta_e}{2}\right] G_M(q^2)^2 \right\} \frac{1}{1-\tau}\,, \tag{12}$$

where: $\tau = q^2/(2M)^2$, θ_e is the lepton scattering angle and $\omega_{1(2)}$ is the energy of the incoming (outgoing) lepton. The expression of eq. (12) is known as the Rosenbluth formula.[8]
The differential cross section for the crossed process of the scattering, i.e. the annihilation $e^+e^- \to N\overline{N}$, in the CM is[9]

$$\frac{d\sigma}{d\cos\theta} = \frac{\pi\alpha^2}{2\,q^2}\beta C_{Q_N}\left[(1+\cos^2\theta)\left|G_M(q^2)\right|^2 + \frac{1}{\tau}\sin^2\theta\left|G_E(q^2)\right|^2\right], \quad \beta = \sqrt{1-\frac{1}{\tau}}\,, \tag{13}$$

where β is the velocity of the outgoing nucleon and C_{Q_N} is the so-called Coulomb factor[10]

$$C_{Q_N} = \begin{cases} \dfrac{\pi\alpha/\beta}{1-\exp(-\pi\alpha/\beta)} & Q_N = 1 \\[2ex] 1 & Q_N = 0\,. \end{cases} \tag{14}$$

It accounts for the electromagnetic $N\overline{N}$ final state interaction and corresponds to the squared value of the Coulomb scattering wave function at the origin.

2. Data and discoveries in the time-like region

The total cross section for production processes: $e^+e^- \to N\overline{N}$ can be obtained from eq. (13) via angular integration and it reads

$$\sigma(e^+e^- \to N\overline{N}) = \frac{4\pi\alpha^2}{3\,q^2}\beta C_{Q_N}\left[\left|G_M(q^2)\right|^2 + \frac{1}{2\tau}\left|G_E(q^2)\right|^2\right]. \tag{15}$$

The cross section of the time-reversed process $N\overline{N} \to e^+e^-$ is related to the previous one through the proportionality relation: $\sigma(N\overline{N} \to e^+e^-) = \sigma(e^+e^- \to N\overline{N})\frac{|\vec{k}_1|^2}{|\vec{p}_1|^2} = \frac{\sigma(e^+e^-\to N\overline{N})}{\beta^2}$, and hence

$$\sigma(N\overline{N} \to e^+e^-) = \frac{4\pi\alpha^2}{3\,q^2}\frac{C_{Q_N}}{\beta}\left[\left|G_M(q^2)\right|^2 + \frac{1}{2\tau}\left|G_E(q^2)\right|^2\right]. \tag{16}$$

Obviously the only difference between the expressions of eq. (15) and (16) lies in the phase-space factor, the dynamical content, represented by the quantity inside the square brackets, is the same.

[a]The Phragmén-Lindelöf theorem states that: given an analytic function $f(z)$, such that $f(z) \to a$ as $z \to \infty$ along a straight line, and $f(z) \to b$ as $z \to \infty$ along another straight line, if $f(z)$ is regular and bounded in the angle between these two lines, then $a = b$ and $f(z) \to a$ uniformly in this angle.

2.1. *The $p\overline{p}$ case*

In order to have comparable data, what usually experiments give is an effective FF obtained under the working hypothesis $|G_E(q^2)| = |G_M(q^2)|$. This assumption is exactly true only at the threshold $q^2 = s_1 = 4M^2$ [see eq. (6)].

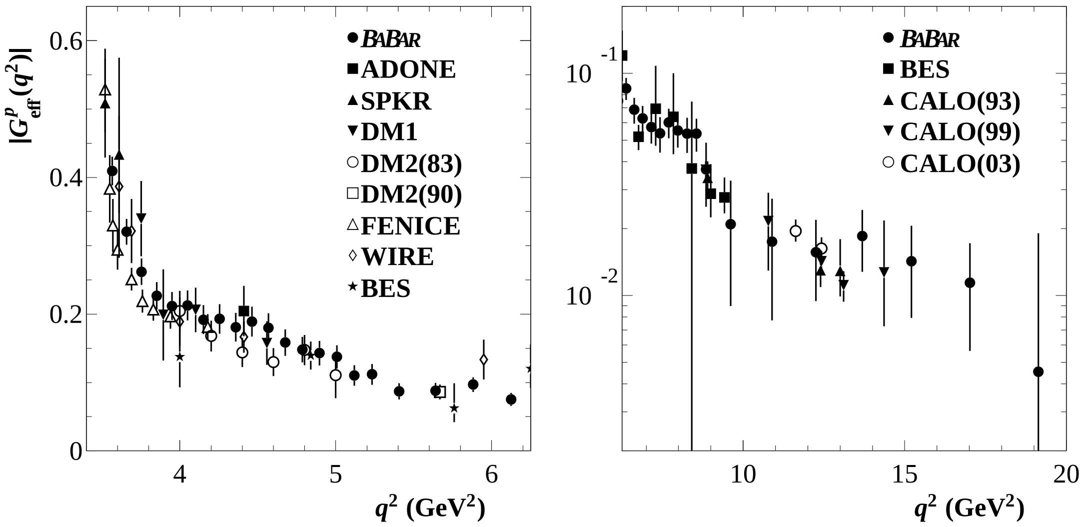

Fig. 5. Worldwide collection of data on $|G^p_{\rm eff}(q^2)|$. The experiments are: B AB AR,[11] ADONE,[12] SPKR,[13] DM1,[14] DM2(83),[15] DM2(90),[16] FENICE,[17] WIRE,[18] BES,[19] CALO(93),[20] CALO(99),[21] CALO(03).[22]

Using the cross section $\sigma(e^+e^- \to p\overline{p})$ from eq. (15) and $\sigma(p\overline{p} \to e^+e^-)$ from eq. (16) in the proton case, i.e. with $N \equiv p$, such an effective FF can be extracted from data through

$$\left|G^p_{\rm eff}(q^2)\right| = \sqrt{\frac{\sigma(e^+e^- \to p\overline{p})}{\dfrac{4\pi\alpha^2}{3q^2}\beta C_1\left(1+\dfrac{1}{2\tau}\right)}} = \sqrt{\frac{\sigma(p\overline{p} \to e^+e^-)}{\dfrac{4\pi\alpha^2}{3q^2}\dfrac{C_1}{\beta}\left(1+\dfrac{1}{2\tau}\right)}}\,, \tag{17}$$

where the second identity holds under the assumption of time-reversal symmetry. In terms of Sachs FFs, $|G^p_{\rm eff}|$ corresponds to the following expression

$$\left|G^p_{\rm eff}(q^2)\right| = \sqrt{\frac{2\tau\left|G_M(q^2)\right|^2 + \left|G_E(q^2)\right|^2}{2\tau+1}}\,. \tag{18}$$

The worldwide collection of data on $|G^p_{\rm eff}|$ is shown in fig. 5. It is interesting to note that at large q^2, even though $|G^p_M| \to |G^p_E|$, the effective FF $|G^p_{\rm eff}|$ goes to $|G^p_M|$.

2.1.1. *Production of $p\overline{p}$ at threshold*

BABAR has measured the cross section of the process

$$e^+e^- \to p\overline{p}$$

with unprecedented accuracy, collecting more then 4000 events in a wide rage of $p\overline{p}$ invariant mass: from threshold up to ~ 4 GeV. The measurement has been performed by using the initial state radiation technique (ISR) and detecting the radiated photon.

Besides the unavoidable drawback to have a reduced luminosity by about a factor of α, the main advantages in using this technique are:

- the detection efficiency is quite high even at the production threshold, i.e. when the $p\overline{p}$-system invariant mass is equal to $2M$. This is a consequence of the fact that the $p\overline{p}$ pair is produced together with a photon and hence it has always a boost in the laboratory frame which makes the detection possible for any $p\overline{p}$ invariant mass;
- an energy resolution of ~ 1 MeV for the hadronic system;
- a full angular acceptance, even at 0^o and 180^o, due to the detection of the radiated photon.

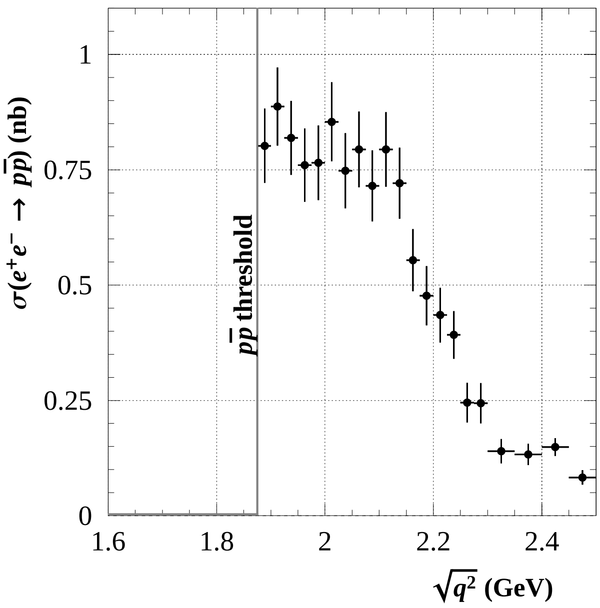

Fig. 6. Low-energy $e^+e^- \to p\overline{p}$ total cross section as measured by BABAR.[11] The gray vertical line indicates the production threshold.

Figure 6 shows low-energy BABAR data on the $e^+e^- \to p\overline{p}$ total cross section. At the production threshold such a cross section is suddenly different from zero and then it maintains an almost constant values for about 200 MeV. At leading order, as $q^2 \to 4M^2$, the behavior of the cross section $\sigma(e^+e^- \to p\overline{p})$, reported in eq. (15), is guided by the phase-space factor and hence it should vanish like the velocity $\beta = \sqrt{1-4M^2/q^2}$. However, since we are producing a pair of charged particles, the Coulomb correction has to be considered. This correction is represented by the factor C_1 defined in eq. (14), that, close to threshold, when $\beta \to 0$, goes like $(\pi\alpha/\beta)$ and then *it compensates the vanishing of the phase-space*. In light of that, the threshold cross section can be computed in terms of the modulus of $G^p(4M^2)$, the common value of G_E^p and G_E^p at $q^2 = 4M^2$ [eq. (6)], and it is[23]

$$\sigma(e^+e^- \to p\overline{p})(4M^2) = \frac{\pi^2\alpha^3}{2M^2} \times \left|G^p(4M^2)\right|^2 = (0.85\,\text{nb}) \times \left|G^p(4M^2)\right|^2 , \tag{19}$$

that, compared with the BABAR threshold measurement[11]

$$\sigma(e^+e^- \to p\overline{p})(4M^2) = 0.85 \pm 0.05\,\text{nb} ,$$

gives the FF normalization:

$$|G^p(4M^2)| = 1.00 \pm 0.05 . \tag{20}$$

This means that the proton and the antiproton, at the production threshold, *behave like a pointlike fermion pair*, i.e. their hadronic structure does not have any effect.

Even though, the identity of eq. (20) corresponds to the normalizations of $G_E^p(q^2)$ and $G_M^p(q^2)/\mu_p$ at $q^2 = 0$, as reported in eq. (7), the validity of similar constraints in the time-like region is completely unexpected. In fact, at that value of q^2, the interpretation of FFs as Fourier transformations of charge and magnetization distributions, which underlies the identities of eq. (7), does not make any sense. Micorscopic models[24] describing nucleon FFs in both space and time-like regions can be easily tuned to fulfil the normalization of eq. (20).

As already pointed out in § 1.1, the hadronic current can be parametrized in terms of different pairs of FFs. Besides $F_{1,2}^p$ and $G_{E,M}^p$, also a partial-wave decomposition can be considered. Indeed, parity conservation allows only $L = 0$ and $L = 2$ angular momentum for the $p\overline{p}$ system, hence we can use the S and D-wave FFs G_S^p and G_D^p. They can be defined as

$$G_S^p = \frac{2G_M^p\sqrt{\tau} + G_E^p}{3} , \qquad G_D^p = \frac{G_M^p\sqrt{\tau} - G_E^p}{3} , \tag{21}$$

and the total cross section of eq. (15), written in terms of G_S^p and G_D^p, becomes

$$\sigma(e^+e^- \to p\overline{p}) = \frac{2\pi\alpha^2}{q^2}\,\frac{\beta}{\tau}\left[C_1\left|G_S^p(q^2)\right|^2 + 2\left|G_D^p(q^2)\right|^2\right] . \tag{22}$$

Here the Coulomb correction C_1 affects the only S wave because the D wave vanishes at the origin.
With a mild assumption on the relative phase between G_E^p and G_M^p, and using the BABAR data on the ratio $|G_E^p|/|G_M^p|$ and total cross section[11] shown in fig. 7, time-like values of $|G_S^p|$ and $|G_D^p|$ can be extracted. Figure 8 shows moduli of S and D-wave FFs, obtained with this procedure in Ref.,[25] and the function $1/\sqrt{\mathcal{R}}$, where $\mathcal{R}$ is the resummation factor of the Coulomb correction. More in detail, the function C_1 defined in eq. (14) is usually written as the product of an enhancement factor $\mathcal{E}$ and a resummation factor $\mathcal{R}$, with

$$\mathcal{E} = \frac{\pi\alpha}{\beta}\,, \qquad \mathcal{R} = \frac{1}{1-\exp(-\pi\alpha/\beta)}\,. \tag{23}$$

BABAR data proved that

$$|G_S^p(q^2)| \simeq \frac{1}{\sqrt{\mathcal{R}}} = \sqrt{1-\exp(-\pi\alpha/\beta)}\,, \qquad \text{for } q^2 \in (4M^2, \sim 4\,\mathrm{GeV}^2)\,,$$

i.e.: the S-wave FF, close to threshold, is in striking agreement with the function $1/\sqrt{\mathcal{R}}$, as it is shown in fig. 8. It follows that, a Coulomb correction, $\widetilde{C}_1$, with the only enhancement factor should imply an S-wave FF, $\widetilde{G}_S^p$, which remains almost constant and equal to one for about 200 MeV above threshold, i.e.

$$C_1 = \mathcal{E}\times\mathcal{R} \;\longrightarrow\; \widetilde{C}_1 = \mathcal{E} \;\Longrightarrow\; |\widetilde{G}_S^p(q^2)| \sim 1\,, \qquad \text{for } q^2 \in (4M^2, \sim 4\,\mathrm{GeV}^2)\,. \tag{24}$$

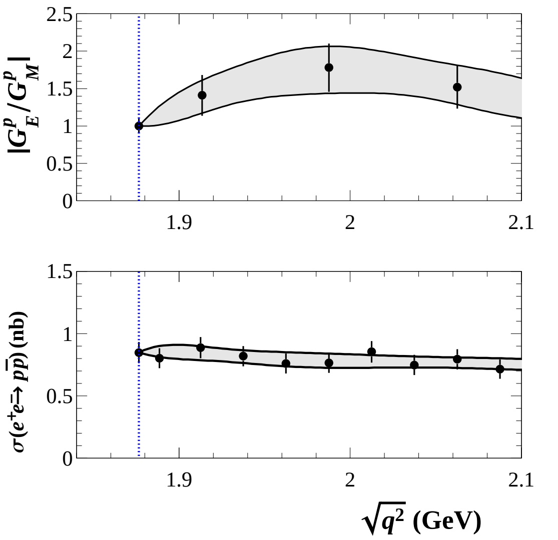

Fig. 7. Top figure: modulus of the ratio $|G_E^p/G_M^p|$; bottom figure: $e^+e^- \to p\overline{p}$ total cross section. The gray bands are the fits, while the dotted vertical line indicates the $p\overline{p}$ production threshold.

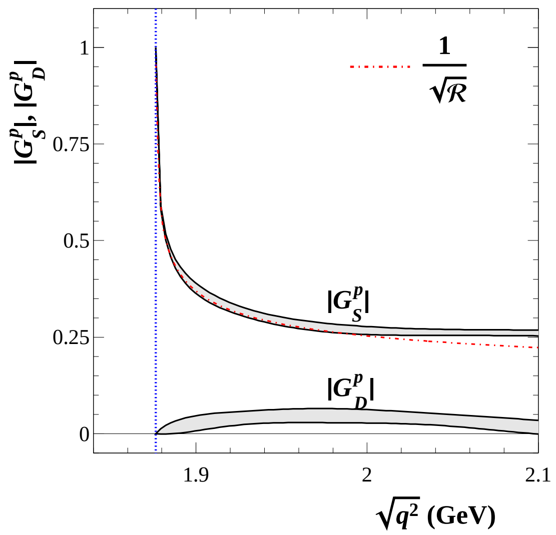

Fig. 8. $|G_S^p|$ and $|G_D^p|$ obtained using the ratio $|G_E^p/G_M^p|$, the total $p\overline{p}$ cross section. The dot-dashed curve is the inverse of the square root of the resummation factor of eq. (23), the dotted line is the $p\overline{p}$ production threshold.

A naïve explanation[25] for the introduction of the "rescaled" factor $\widetilde{C}_1$ of eq. (24) could be the existence of a cutoff for the Coulomb dominance that, in case of baryons, is hundred times greater than that expected for pointlike charged fermions.

2.2. *The ratio $|G_E^p/G_M^p|$*

For the first time BABAR has measured the modulus of the ratio between electric and magnetic FFs in the annihilation $e^+e^- \to p\overline{p}$. There exists only one previous attempt done by the WIRE Collaboration, but in the time-reversed process $p\overline{p} \to e^+e^-$.[18] Recently, performing a re-analysis of old data sets from; the e^+e^- experiments FENICE and DM2, and the $p\overline{p}$ experiment E835, two new points have been added.[26] Figure 9 shows all available data in the time-like region for the modulus of the ratio

$$R(q^2) = \mu_p\,\frac{G_E^p(q^2)}{G_M^p(q^2)}\,. \tag{25}$$

The horizontal line represents the so called "scaling", i.e. the identity $|G_E^p| = |G_M^p|$, that, in principle, holds only at the threshold, see eq. (6), where not only moduli but also phases coincide. In particular the validity of the scaling above threshold has been definitively disproved by *BABAR* (fig. 9) that measured for the first time the inequality

$$|G_E^p(q^2)| > |G_M^p(q^2)|\,, \qquad \text{for } q^2 \sim 2\,\mathrm{GeV}^2\,. \tag{26}$$

From the theoretical point of view the ratio $R(q^2)$ is an analytic function in the whole q^2-complex plane with the cut (s_0, ∞), as each single FFs (see § 1.2), it follows that its time-like and space-like values are intimately related. In particular, the time-like enhancement has been connected with the space-like data that show, instead, a decreasing behavior.[27]
Furthermore, time-like data on $|R|$ can be used to estimate the two-photon contribution in the process $e^+e^- \to p\overline{p}$. Indeed, the two-photon exchanged annihilation $e^+e^- \to \gamma^*\gamma^* \to p\overline{p}$ has positive charge conjugation, $C = +1$, hence its amplitude interferes with the $C = -1$ Born amplitude, originating terms with odd powers of $\cos\theta$ in the angular distribution. A study performed on the *BABAR* data gave an estimate for two-photon exchange contribution of the order of few %,[28] in agreement with natural expectations for radiative corrections.

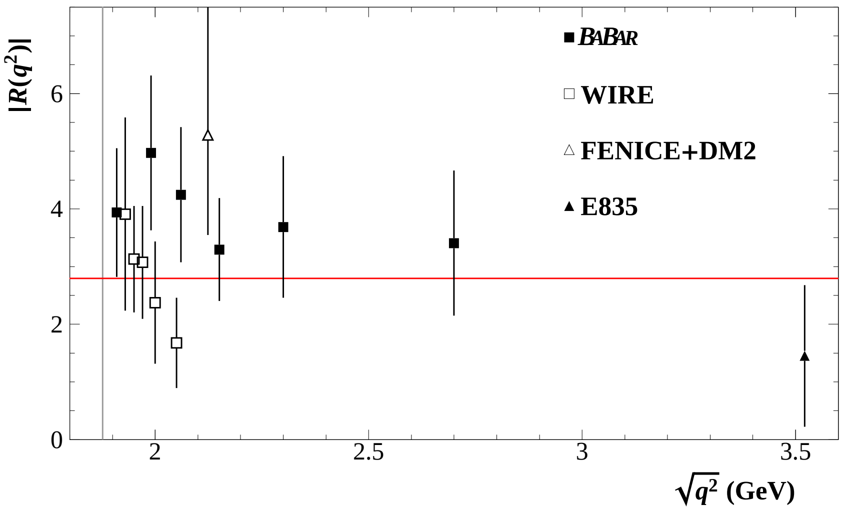

Fig. 9. Modulus of the ratio $R = \mu_p G_E^p / G_M^p$. *BABAR* data[11] (solid squares) are compared with WIRE[18] data (empty squares) and two other points obtained from reanalyses of old data sets (triangles). The horizontal line indicates the identity $|G_E^p| = |G_M^p|$, i.e. $R = \mu_p$, while the vertical line is the threshold.

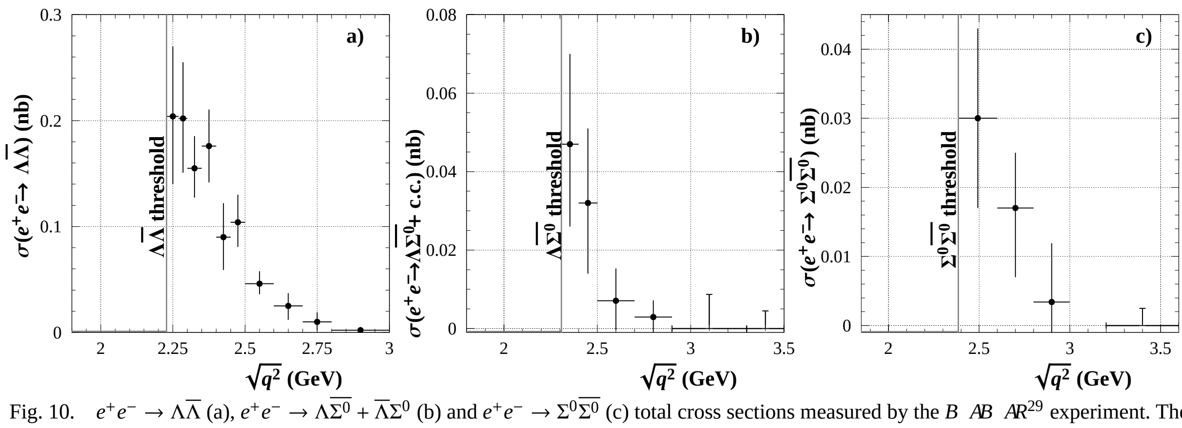

Fig. 10. $e^+e^- \to \Lambda\overline{\Lambda}$ (a), $e^+e^- \to \Lambda\overline{\Sigma^0} + \overline{\Lambda}\Sigma^0$ (b) and $e^+e^- \to \Sigma^0\overline{\Sigma^0}$ (c) total cross sections measured by the *BABAR*[29] experiment. The gray vertical lines indicate the production thresholds.

2.3. *Strange baryons*

The peculiar behavior shown by the $e^+e^- \to p\overline{p}$ process, i.e. a cross section which is suddenly different from zero at threshold where it reaches its maximum value and then decreases uniformly, has been observed also in other reactions where baryon-

antibaryon pairs are produced via e^+e^- annihilation. BABAR measured total cross sections for the processes: $e^+e^- \to \Lambda\overline{\Lambda}$, $e^+e^- \to \Lambda\overline{\Sigma^0} + \overline{\Lambda}\Sigma^0$ and $e^+e^- \to \Sigma^0\overline{\Sigma^0}$ using the ISR technique,[29] in particular $\sigma(e^+e^- \to \Lambda\overline{\Sigma^0} + \overline{\Lambda}\Sigma^0)$ and $\sigma(e^+e^- \to \Sigma^0\overline{\Sigma^0})$ have been measured for the first time, while for $\sigma(e^+e^- \to \Lambda\overline{\Lambda})$ there exists only one previous data point from the DM2 collaboration.[16]
Figure 10 shows the cross section data that, even if with larger errors, have the same trend as the $p\overline{p}$ data. The interesting thing is that in all these processes the involved baryons are neutral and hence no "standard" Coulomb correction is expected. A possible explanation, still based on the copositness of the baryons, could be that threshold behaviors are due to remnants of Coulomb interactions but at quark level.[25]
A study of these strange baryon FFs using U-spin[30] relationships, and hence flavor-$SU(3)$ invariance also in the low-q^2 region, could be justified by their small mass differences. In particular, assuming negligible electromagnetic transitions between U-spin triplet and singlet, one can set the following relation among magnetic moments

$$\mu_\Lambda = \mu_{\Sigma_0} + \frac{2}{\sqrt{3}}\mu_{\Lambda\overline{\Sigma^0}}$$

that could be interpreted as the FF normalization

$$G_\Lambda = G_{\Sigma_0} + \frac{2}{\sqrt{3}}G_{\Lambda\overline{\Sigma^0}},$$

that should hold at least at some q^2 value. In the time-like region at the production threshold the electric and magnetic FFs coincide and are exactly proportional to the square root of the cross section, hence, at this momentum transferred, the previous relationship can be written in terms of masses and cross sections as

$$M_\Lambda\sqrt{\sigma_{\Lambda\overline{\Lambda}}} = M_{\Sigma_0}\sqrt{\sigma_{\Sigma^0\overline{\Sigma^0}}} + \frac{2}{\sqrt{3}}\overline{M}_{\Lambda\Sigma_0}\sqrt{\sigma_{\Lambda\overline{\Sigma^0}}}.$$

If we use threshold values extrapolated from the lowest energy point of the three BABAR data sets shown in fig. 10, we can check this identity by evaluating the ratio

$$\frac{\left|M_\Lambda\sqrt{\sigma_{\Lambda\overline{\Lambda}}} - M_{\Sigma_0}\sqrt{\sigma_{\Sigma^0\overline{\Sigma^0}}} - (2/\sqrt{3})\overline{M}_{\Lambda\Sigma_0}\sqrt{\sigma_{\Lambda\overline{\Sigma^0}}}\right|}{M_\Lambda\sqrt{\sigma_{\Lambda\overline{\Lambda}}} + M_{\Sigma_0}\sqrt{\sigma_{\Sigma^0\overline{\Sigma^0}}} + (2/\sqrt{3})\overline{M}_{\Lambda\Sigma_0}\sqrt{\sigma_{\Lambda\overline{\Sigma^0}}}} = 0.01 \pm 0.10\,. \qquad (27)$$

Despite the large error due the low statistics of the data, this result is impressive. In fact, the connection among the threshold values of these quite different cross sections (the data are spread in a wide range, from tens to hundreds of picobarns) is incredibly good.
However, vanishing cross sections at threshold, raising according to the baryon velocity phase space factor, cannot be excluded by the present BABAR data.[25] More precise measurements are needed to settle this issue.
Furthermore, in the case of $\Lambda\overline{\Lambda}$ production there is the unique opportunity to access the complex structure of the Λ electric and magnetic FFs. Indeed, studying the angular distribution of the decay $\Lambda \to p\pi^-$ ($\overline{\Lambda} \to \overline{p}\pi^+$) it is possible to measure the Λ ($\overline{\Lambda}$) polarization, whose component perpendicular to the scattering plane is proportional to the sine of the relative phase between G_E^Λ and G_M^Λ.[31] A first attempt to determine this phase has been done,[29] but the limited statistics did allow only a poor estimate.

Figure 11 shows data on the $e^+e^- \to n\overline{n}$ total cross section. There are only two measurements; the first one done in 1993 by the FENICE Collaboration in Frascati[32] and a more recent set obtained in 2011 by the SND experiment[33] at the VEPP-2000 collider in Novosibirsk. The red curve is a fit of the first four data points done using a dipole-type effective FF, with two free parameters.
Even though there are no well establish predictions for such a cross section, the obtained values appear quit high. Indeed, by using as $n\overline{n}$ effective FF the measured $p\overline{p}$ one, scaled by the ratio between d and u quark charges, we get an estimate for such a cross section, the blue curve of fig. 11, which, close to threshold, is at least a factor of four lower than the data.

3. Conclusions

The knowledge, the study and the comprehension of baryon FFs are indispensable steps towards a deep understanding of the low-energy QCD dynamics. Nevertheless, even in case of nucleons, the available data are still quite incomplete. The experimental situation is twofold:

- many data sets in the space-like region where recently, with the increasingly common use of polarization techniques (see e.g.[34]), a great improvement of accuracy and hence of the capability to disentangle electric and magnetic FFs has been achieved;

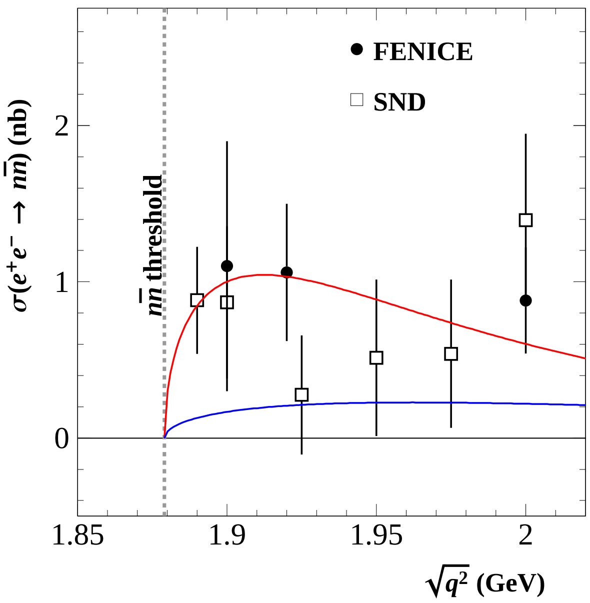

Fig. 11. Total cross section of $e^+e^- \to n\bar{n}$ measured by FENICE[32] and SND.[33] The gray vertical line indicates the production threshold, the red curve is the fit described in the text and the blue curve represents the naïve expectation driven from the $p\bar{p}$ data.

- few measurements in the time-like region, with only two attempts, which actually gave incompatible results, to separate the moduli of G_E and G_M for the proton.

From the theoretical point of view, different interpretations have been proposed and the wide variety of attempts reflects the difficulty to connect the phenomenological properties of nucleons, parametrized by the FFs, to the underlying theory which is the QCD in non-perturbative (low-energy) regime.
Nevertheless, the analyticity requirement, which compels descriptions to be valid in both space- and time-like regions, drastically reduces the range of models to be considered. In particular, the more successful ones are the Vector-Meson-Dominance based models,[35] that not only are easily extensible from negative to positive q^2, but they were also able to make quite "unnatural" predictions then confirmed by the data. An example is the Iachello-Jackson-Landé model,[36] the authors predicted in 1973 the decreasing space-like behavior for the ratio G_E^p/G_M^p well 30 years before its experimental observation.[37]
BABAR data gave a factual help in shedding light on the time-like behavior of proton FFs. Three very interesting aspects have been clarified:

- the threshold unitary normalization for the proton FF, see eq. (20);
- the need of a rescaled Coulomb correction accounting for the structure of baryons;
- the inequality of eq. (26): $|G_E^p(q^2)| > |G_M^p(q^2)|$, just above the production threshold.

Many other aspects of the time-like FFs, i.e.: a separate extraction of $|G_E|$ and $|G_M|$, the measurement of their relative phase, the explanation of the threshold normalization and the asymptotic behavior in connection with the space-like region, are still waiting for further experimental results and theoretical interpretations.

Acknowledgments

We owe a special thanks to the Organizers of the "2011 Ferrara International School Niccolò Cabeo on Hadron Structure and Interactions" and, for suggestions and fruitful discussions on the topics of this work, we acknowledge Guido Altarelli, Giulia Pancheri, Yogendra Srivastava and Antonino Zichichi.

References

1. L. L. Foldy, Phys. Rev. **87**, 688 (1952).
2. L. N. Hand, D. G. Miller and R. Wilson, Rev. Mod. Phys. **35**, 335 (1963).
3. M. Gell-Mann, M. L. Goldberger and W. E. Thirring, Phys. Rev. **95**, 1612 (1954);
M. L. Goldberger, Phys. Rev. **97**, 508 (1955).

4. G. F. Chew, R. Karplus, S. Gasiorowicz, and F. Zachariasen, Phys. Rev. **110**, 265 (1958);
P. Federbush, M. L. Goldberger, and S. B. Treiman, Phys. Rev. **112**, 642 (1958).
5. S. J. Brodsky and G. R. Farrar, Phys. Rev. Lett. **31**, 1153 (1973);
V. Matveev *et al.*, Nuovo Cimento Lett. **7** (1973) 719.
6. G. P. Lepage and S. J. Brodsky, Phys. Rev. D **22**, 2157 (1980).
7. L. E. Phragmén, and E. Lindelöf, Acta Math. **31**, 381 (1908);
E. C. Tichmarsch, *The Theory of Functions* (Oxford University Press, London, 1939).
8. M. N. Rosenbluth, Phys. Rev. **79**, 615 (1950).
9. A. Zichichi, S. M. Berman, N. Cabibbo and R. Gatto, Nuovo Cim. **24** (1962) 170.
10. A. D. Sakharov, Zh. Eksp. Teor. Fiz. **18**, 631 (1948) [Sov. Phys. Usp. **34**, 375 (1991)];
A. Sommerfeld, *Atombau und Spektralliniem* (Vieweg, Braunschweig, 1944), Vol. 2, p.130;
J. Schwinger, *Particles, Sources, and Fields* (Addison-Wesley, Reading, Massachusetts, 1973), Vol. III, p. 80.
11. B. Aubert *et al.* [BABAR Collaboration], Phys. Rev. D **73**, 012005 (2006) [arXiv:hep-ex/0512023].
12. M. Castellano, G. Di Giugno, J. W. Humphrey, E. Sassi Palmieri, G. Troise, U. Troya and S. Vitale, Nuovo Cim. A **14**, 1 (1973).
13. G. Bassompierre *et al.*, Phys. Lett. B **64**, 475 (1976).
14. B. Delcourt *et al.*, Phys. Lett. B **86**, 395 (1979).
15. D. Bisello *et al.* [DM2 Collaboration], Nucl. Phys. B **224**, 379 (1983).
16. D. Bisello *et al.* [DM2 Collaboration], Z. Phys. C **48**, 23 (1990).
17. A. Antonelli *et al.*, Phys. Lett. B **334**, 431 (1994).
18. G. Bardin *et al.*, Nucl. Phys. B **411**, 3 (1994).
19. M. Ablikim *et al.* [BES Collaboration], Phys. Lett. B **630**, 14 (2005) [arXiv:hep-ex/0506059].
20. T. A. Armstrong *et al.* [E760 Collaboration], Phys. Rev. Lett. **70**, 1212 (1993).
21. M. Ambrogiani *et al.* [E835 Collaboration], Phys. Rev. D **60**, 032002 (1999).
22. M. Andreotti *et al.*, Phys. Lett. B **559**, 20 (2003).
23. R. Baldini, S. Pacetti, A. Zallo and A. Zichichi, Eur. Phys. J. A **39**, 315 (2009) [arXiv:0711.1725 [hep-ph]]; R. B. Baldini, S. Pacetti and A. Zallo, arXiv:0812.3283 [hep-ph].
24. E. A. Kuraev, E. Tomasi-Gustafsson and A. Dbeyssi, arXiv:1106.1670 [hep-ph].
25. R. B. Ferroli, S. Pacetti and A. Zallo, arXiv:1008.0542 [hep-ph].
26. R. Baldini, C. Bini, P. Gauzzi, M. Mirazita, M. Negrini and S. Pacetti, Nucl. Phys. Sec. A **755**, 286 (2005); R. Baldini, C. Bini, P. Gauzzi, M. Mirazita, M. Negrini and S. Pacetti, Eur. Phys. J. C **46**, 421 (2006).
27. S. Pacetti, Eur. Phys. J. A **32**, 421 (2007)
28. E. Tomasi-Gustafsson, E. A. Kuraev, S. Bakmaev and S. Pacetti, Phys. Lett. B **659**, 197 (2008) [arXiv:0710.0454 [hep-ph]].
29. B. Aubert *et al.* [BABAR Collaboration], Phys. Rev. D **76**, 092006 (2007) [arXiv:0709.1988 [hep-ex]].
30. D. Park, *Introduction to strong interactions* (W. A. Benjamin, Inc., New York, 1966).
31. A. Z. Dubničkova, S. Dubnička, M. P. Rekalo, Nuovo Cim. A **109**, 241 (1996).
32. A. Antonelli *et al.*, Nucl. Phys. B **517**, 3 (1998).
33. S. I. Serednyakov, "First results from SND at VEPP-2000", *International Workshop on e^+e^- collisions from Phi to Psi*, BINP, Novosibirsk, 2011.
34. C. F. Perdrisat, V. Punjabi and M. Vanderhaeghen, Prog. Part. Nucl. Phys. **59**, 694 (2007) [arXiv:hep-ph/0612014].
35. See e.g. E. Tomasi-Gustafsson, F. Lacroix, C. Duterte and G. I. Gakh, Eur. Phys. J. A **24**, 419 (2005) [arXiv:nucl-th/0503001].
36. F. Iachello, A. D. Jackson and A. Landé, Phys. Lett. B **43** (1973) 191.
37. M. K. Jones *et al.* [Jefferson Lab Hall A Collaboration], Phys. Rev. Lett. **84**, 1398 (2000) [arXiv:nucl-ex/9910005];
O. Gayou *et al.*, Phys. Rev. C **64**, 038202 (2001);
O. Gayou *et al.* [Jefferson Lab Hall A Collaboration], Phys. Rev. Lett. **88**, 092301 (2002) [arXiv:nucl-ex/0111010];
A. J. R. Puckett *et al.*, Phys. Rev. Lett. **104**, 242301 (2010) [arXiv:1005.3419 [nucl-ex]];
B. D. Milbrath *et al.* [Bates FPP collaboration], Phys. Rev. Lett. **80**, 452 (1998) [Erratum-ibid. **82**, 2221 (1999)] [arXiv:nucl-ex/9712006].